Pergamon

International Journal of Machine Tools & Manufacture 42 (2002) 905–913

INTERNATIONAL JOURNAL OF
MACHINE TOOLS
& MANUFACTURE
DESIGN, RESEARCH AND APPLICATION

A revisit to some wheel–workpiece interaction problems in surface grinding

I. Zarudi, L.C. Zhang *

School of Aerospace, Mechanical and Mechatronic Engineering, The University of Sydney, Sydney, NSW 2006, Australia

Received 22 January 2002; accepted 12 February 2002

Abstract

This paper revisited some wheel–workpiece interaction problems in surface grinding including the profile of heat flux and the variation of the wheel's elastic modulus. A method of using an optical microscope and a CCD camera was applied to capture the depth and width of the heated zone, the details of the temperature field and the stability of the heat flux. It was found that the heat flux in up-grinding can be modeled as a triangle with its apex at the inlet of the wheel–workpiece contact arc. The elastic modulus of the grinding wheel decreases significantly when the grinding temperature is beyond a critical value and can be described by a power law. It was also found that the depth of cut has almost no effect on the partition of the grinding energy. © 2002 Elsevier Science Ltd. All rights reserved.

Keywords: Heat flux; Surface grinding; Temperature field; Elastic modulus

1. Introduction

In a previous study [1], the authors reported that the beneficial microstructure formed in surface grinding is the result of the special temperature-stress field generated by the wheel–workpiece interaction. Hence, an accurate prediction of the grinding-induced temperature rise is of primary importance to control the formation of such advantageous microstructure. This involves an in-depth understanding of the heat flux profile and the mechanical and thermal deformation of both the workpiece and grinding wheel in the grinding zone.

A number of studies have tried to evaluate the heat flux profile in conventional and creep-feed grinding [2–10]. The heat flux has been modeled in various ways—as a uniform [2,3], triangular [4, 5, 7–9], parabolic [10] or a complex profile along the grinding zone [11]. The uniform heat flux model [2,3] led to an evident contradiction in matching the temperature experimentally measured as pointed out by Jen and Lavine [11,12]. Rowe [10] considered the effect of the variable thickness of an underformed chip in grinding and proposed a parabolic heat flux distribution based on his experimental findings. However, by taking into account the contact deformation between a grinding wheel and a workpiece, Zhang and co-authors [8] showed that the heat flux should be neither rectangular nor parabolic but triangular. They concluded that the surface heat generated had a close relationship with the local deformation of the workpiece material in contact with the grinding wheel. A high local temperature rise related to a significant local plastic deformation of the workpiece and a high local intensity of the interface forces. It was found that the prediction of a triangular heat flux model was in good agreement with experimental measurements [9]. Further investigations considering the influence of the apex position of the triangular heat flux were also carried out [6,7]. It was admitted that the temperature field in the grinding zone could vary considerably when the apex was shifted.

The experimental studies specified above used a thermocouple technique to measure the temperature rise in the subsurface of a component subjected to grinding [9,10]. However, the technique implies a number of limitations and the position of the flux apex could not be located with a satisfactory resolution [13]. Furthermore, the distance between the thermocouple and the wheel in a grinding pass can be only estimated at an accuracy of

* Corresponding author. Tel.: +61-2-9351-2835; fax: +61-2-9351-7060.

E-mail address: zhang@mech.eng.usyd.edu.au (L.C. Zhang).

PII: S0890-6955(02)00024-X

Table 1
The chemical composition of the AISI 4140 steel

Chemical element	Fe	C	Si	Mn	Cr	Mo
%	Balance	0.40	0.25	0.80	0.90	0.20

Table 2
Grinding conditions

Grinding mode	Up-grinding
Workpiece material	Steel 4140
Grinding wheel	A120MVAA
Wheel diameter (mm)	280
Wheel speed (m/s)	17
Grinding width (mm)	15
Table speed (m/min)	0.02, 0.05, 0.1, 0.2, 0.3
Depth of cut (μm)	35, 70, 105

a half depth of cut. This results in an inadequate measurement resolution when the depth of cut is large. In addition, multi-passes are required to obtain the temperature distribution in the subsurface of a workpiece, but identical grinding conditions in individual passes, such as the wheel surface conditions, cannot be guaranteed.

The present study will investigate the grinding heating by an alternative method that avoids the drawbacks of the thermocouple technique. An optical microscope and a CCD camera will be used to attain a sufficient space resolution and temperature field distribution in a single grinding pass. This will make it possible to carry out a more comprehensive analysis on the contact deformation, thermal deformation of the workpiece and the change of the wheel's elastic modulus.

2. Experiment

The testing material selected was a widely used steel, AISI 4140, initially tempered. The chemical composition of the steel is listed in Table 1.

Up-grinding was performed on a surface grinder, Minini Junior 90 CF CNC M286, with the grinding parameters listed in Tables 2 and 3 (Fig. 1). A three-component 'Kistler' dynamometer of type 9257B was used to measure the grinding forces.

A temperature measuring system composed of an optical microscope, a CCD camera and a video recorder were constructed as shown in Fig. 2. The profile of the heated zone by this method can be obtained when the temperature rise in the subsurface exceeds 550 °C. The temperature field was then analyzed by an image analysis system, Leica Qwin, with the aid of a color chart.

Table 3
Wheel dressing conditions

Type of dresser	single-point diamond
Wheel speed (m/min)	10
Dressing, cross-feed rate (mm/revolution)	0.1

The depth of the heat-affected layer in a ground workpiece was checked on the cross-section view samples by means of an optical microscope. The profile of a grinding wheel surface was studied by a scanning electron microscope (JEOL 505).

Wear flats of the grinding wheel were assessed by a Laser Scanning Confocal Imaging System MRC-600. In this study, the wear flats were approximated as the intersection areas of the abrasives exposed on the grinding wheel surface with a horizontal scanning plane. To take into account the variation of the wear flats when the depth of cut changed, the distance between the scanning plane and the highest point of the grinding wheel was varied to reflect the effect of the depth of cut (see Fig. 3 for details).

3. Results and discussion

3.1. The heated zone

3.1.1. Experimental observations

The experimentally observed heated zones in a workpiece and grinding wheel are shown in Fig. 4. Under all the grinding conditions tested, the maximum temperature rise did not appear at the outlet point of the wheel–workpiece contact, which indicates that the uniform heat flux model is inconsistent with experiment.

The experiment showed that the profiles of the heated zone in the workpiece and grinding wheel are asymmetric about the center of the grinding zone (Fig. 4). The workpiece material has a higher conductivity and thus has a much deeper heat penetration depth. The maximum temperature was at the wheel–workpiece contact interface. In the following discussion, for convenience, it is assumed that the heated zones are bounded by 800 °C, the temperature for α–γ phase transformation. The increase in the depth of cut leads to a greater heated zone with its width and depth both growing as detailed in Table 4. This is reasonable because there is a higher energy input in grinding when the depth of cut increases.

The infeed velocity affects the dimension of the

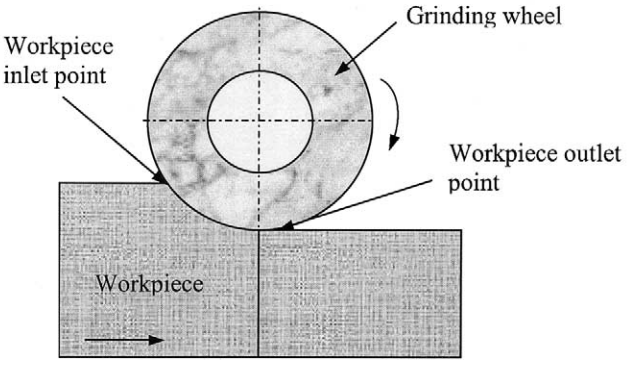

Fig. 1. Schematic diagram of an up-grinding.

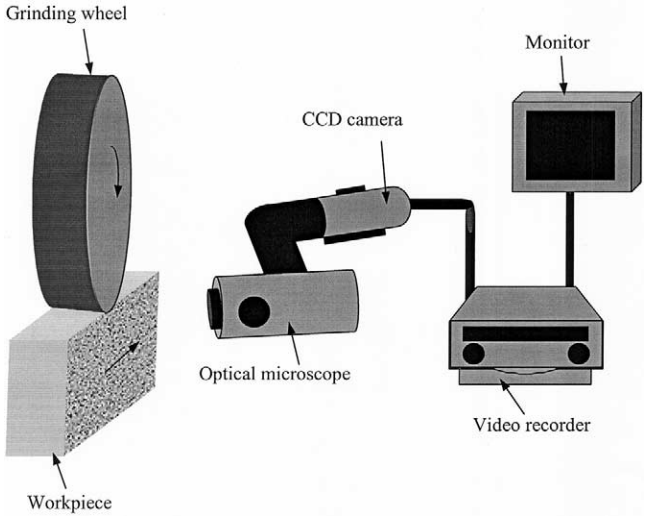

Fig. 2. The temperature field recording system.

heated zone in a complicated manner. Initially, an increase of the infeed velocity leads to a larger heated zone (Table 4). However, when it increases further, the development of the zone size becomes non-monotonic. The shrinkage of the zone could be due to the decreasing heating time when the infeed velocity was large, as in this case the heat source on the workpiece surface moved faster and less amount of heat could actually conduct into the workpiece.

3.1.2. Theoretical prediction

Jaeger's model of a moving heat source [14] was used to calculate the heated zone theoretically. The surface heat flux was modeled as a triangle. Two variables were considered, the base length (contact length in grinding) and the apex position. As the base length can deviate significantly from the geometrical contact length at high grinding loads [14], the grinding with a low depth of cut was first studied to minimize the effect. In this way we

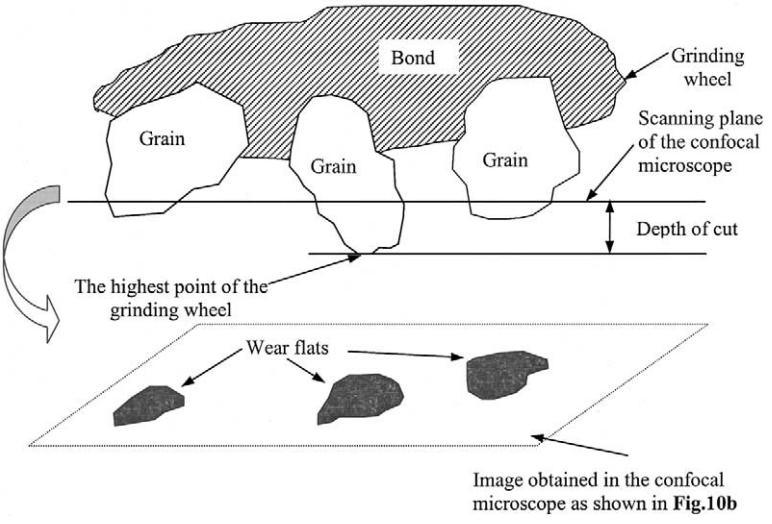

Fig. 3. Schematic diagram of wheel's wear flats measurements using a confocal scanning microscope.

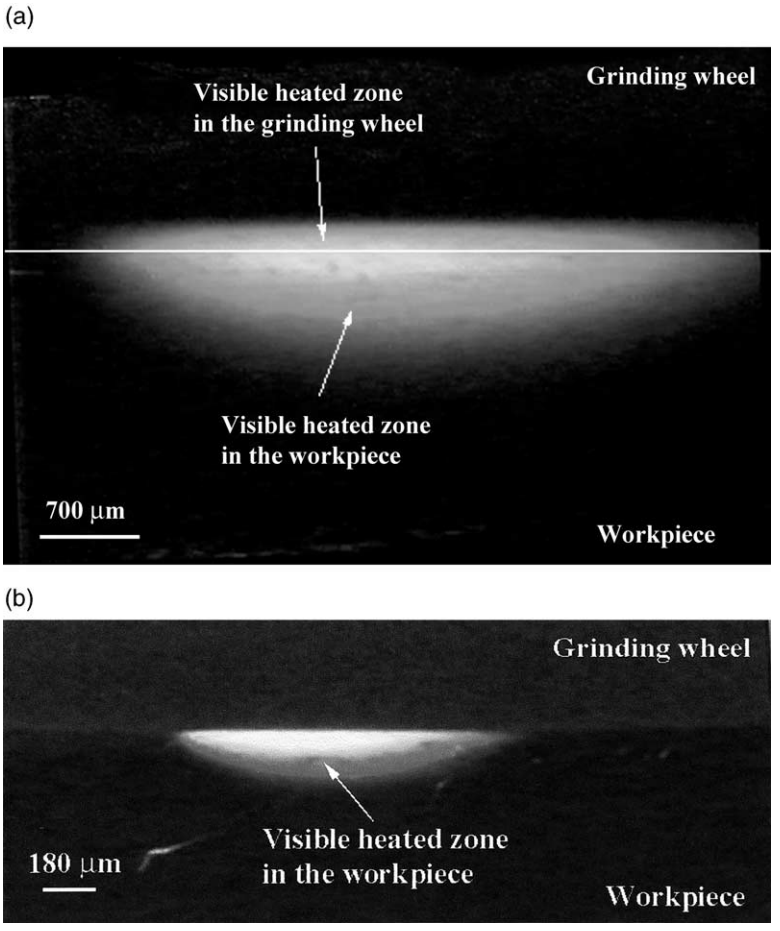

Fig. 4. Effect of the infeed velocity on the heated zone profile at depth of cut of 70 μm. (a) Infeed velocity=0.1 m/min; (b) infeed velocity=0.02 m/min.

Table 4
Effect of the grinding variables on the stability and dimensions of the heated zone

Grinding regimes		Depth of the heat-affected layer (μm)	Duration of flashing (s)	Time between flashes (s)	Width of the heated zone (mm)	Depth of the heated zone (μm)	Average roughness Ra (μm)
Depth of cut (μm)	Infeed velocity (m/min)						
35	0.02	0	0	N/A	0	0	0.24
	0.05	130	0.06	0.33	1.73	140	0.51
	0.1	460	0.1	0.29	2.2	420	0.62
	0.2	500	0.15	0.09	2.4	460	0.35
	0.3	580	Pulsating	0	2.8	530	0.32
70	0.02	180	0.13	1.1	2.3	180	0.43
	0.05	350	0.14	0.24	2.60	400	0.75
	0.1	650	0.19	0.14	4.10	640	0.38
	0.2	880	Pulsating	0	5.20	840	0.20
	0.3	690	Continuous	0	4.50	720	0.24
105	0.02	300	0.056	1.09	2.45	230	0.51
	0.05	740	0.10	0.3	4.5	650	0.43
	0.1	830	Pulsating	0	5.3	800	0.25
	0.2	1000	Continuous	0	6.10	950	0.28
	0.3	900	Continuous	0	5.40	840	0.21

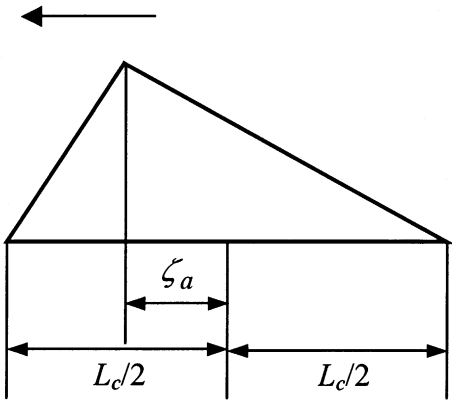

Fig. 5. A theoretical triangular model of the heat flux.

can uncover the influence of the apex position in grinding.

The apex position of a heat flux is defined in Fig. 5 as

$$l_a = \frac{2\zeta_a}{L_c} \quad (1)$$

where L_c is the base length of the heat flux and is the distance from the apex to the center of the flux. The effect of the apex position on the heated zone profile is shown in Fig. 6, which demonstrates that l_a=1 gives rise to the best fit between the experimental and theoretical profiles. Dimensions of the experimental and theoretical heated zones under various grinding conditions are presented in Fig. 7. Again l_a=1 gives the best correlations with the experimental measurements.

3.2. Stability of the heated zone

The instability of a heated zone was an interesting event observed. At a low infeed velocity (e.g., from 0.02 to 0.1 m/min) the heated zone did not appear continuously but flashed (see Table 4). Physically, the flashing indicates that the grinding-heating was unstable and the temperature in the workpiece was often below the optically observable value. With the increase of the infeed velocity (e.g. from 0.1 to 0.2 m/min) the heated zone could be observed continuously although its depth still varied. The zone became stable only when the infeed velocity became sufficiently large (e.g. 0.2–0.3 m/min). In addition, the increase of the depth of cut promotes the stability of the heated zone at low infeed velocities.

The instability of heating is undesirable as it made the grinding-induced layer uneven and the integrity of the ground material poor, as shown in Fig. 8 and Table 4. The instability also affects the surface roughness of a ground component. The average roughness varied from 0.3 to 0.8 μm under an unstable heating. More significantly, it generated harmful surfaces (Fig. 9a). A stable heating produced an average roughness of about 0.25 μm and led to a normal surface quality (Fig. 9b).

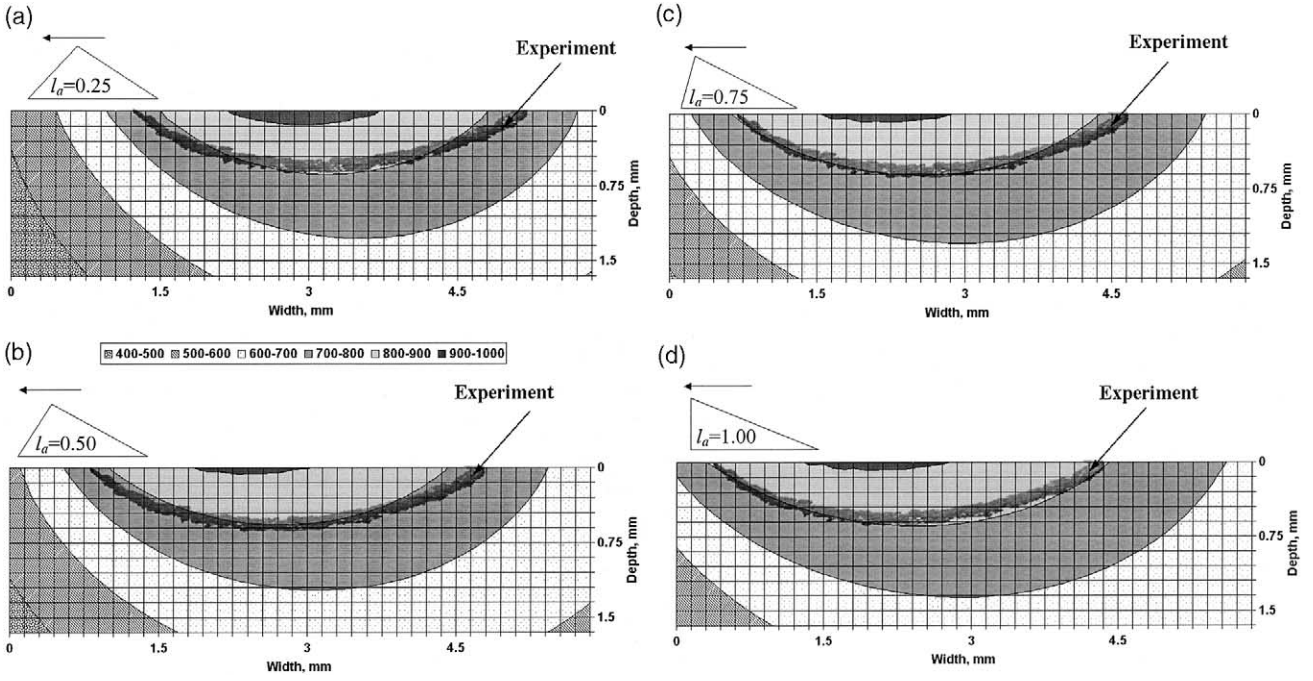

Fig. 6. A comparison of the experimentally recorded heated zone and theoretical temperature field (depth of cut=70 μm and infeed velocity=0.1m/min). (a) l_a=0.25; (b) l_a=0.5; (c) l_a=0.75; (d) l_a=1.

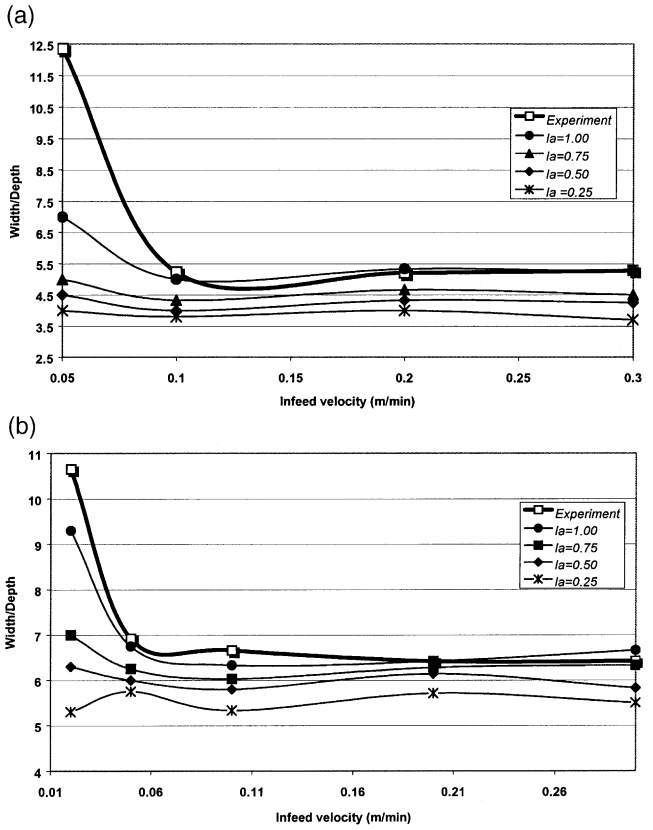

Fig. 7. The effect of the grinding variables on the threshold of width/depth of the heated zones. (a) Depth of cut=35 μm; (b) depth of cut=105 μm.

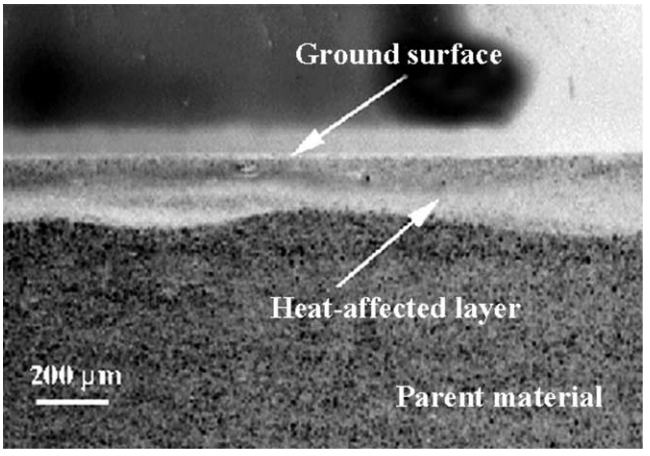

Fig. 8. An uneven grinding-induced layer due to an unstable heating (depth of cut=35 mm, infeed velocity=0.05 m/min).

3.3. Wear flats and energy partition

The general view of the grinding wheel topography is demonstrated in Fig. 10a. The alumina abrasives are irregular in shape and have rather sharp edges. In addition the grinding wheel features a rather porous structure. The variation of the wear flats of the wheel is presented in Fig. 10b and Table 5. The increase of the depth of cut alters the area of the wear flats very slightly.

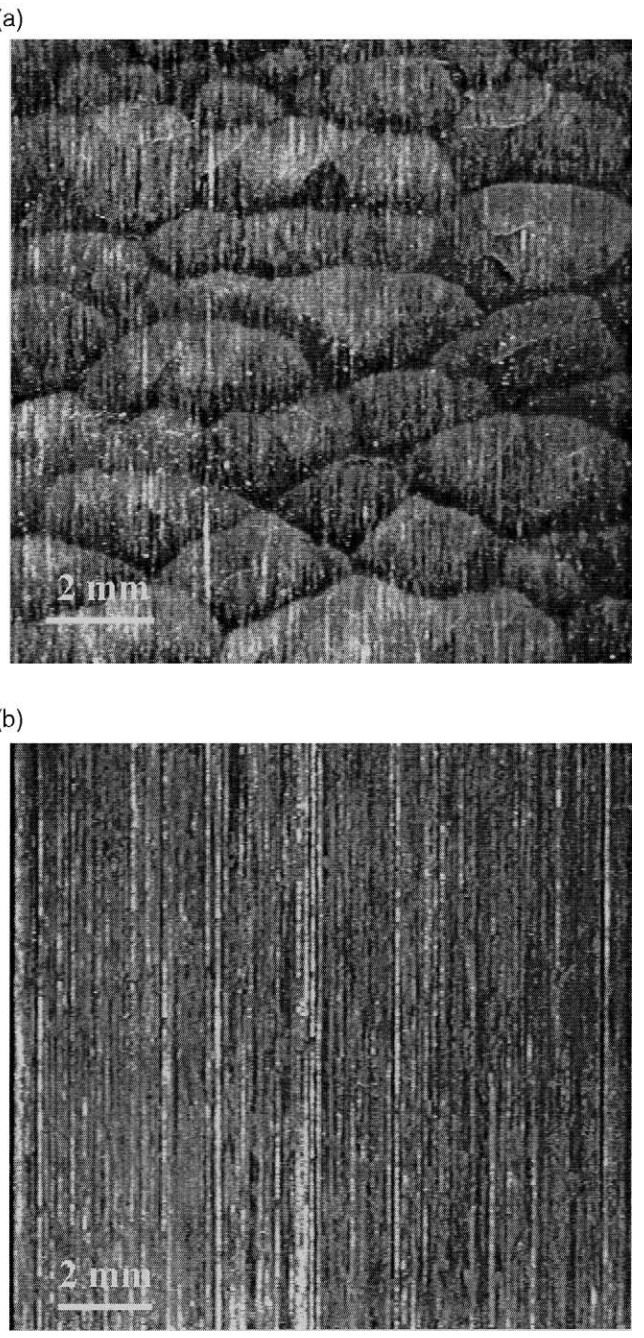

Fig. 9. The surface topography after grinding at depth of cut of 35 μm. (a) Infeed velocity=0.05 m/min. Note the uneven surface due to the unstable heating. (b) Infeed velocity=0.3m/min. Note the normal surface features introduced by grinding. In this case the heating is stable.

The energy partition to the workpiece, R_{ws}, can be obtained using the grain contact model [15], i.e.,

$$R_{ws} = \frac{1}{1 + \dfrac{k_{ge}}{\sqrt{r_0 v_s}} \times \dfrac{1}{\sqrt{(k\rho c)_w}}} \tag{2}$$

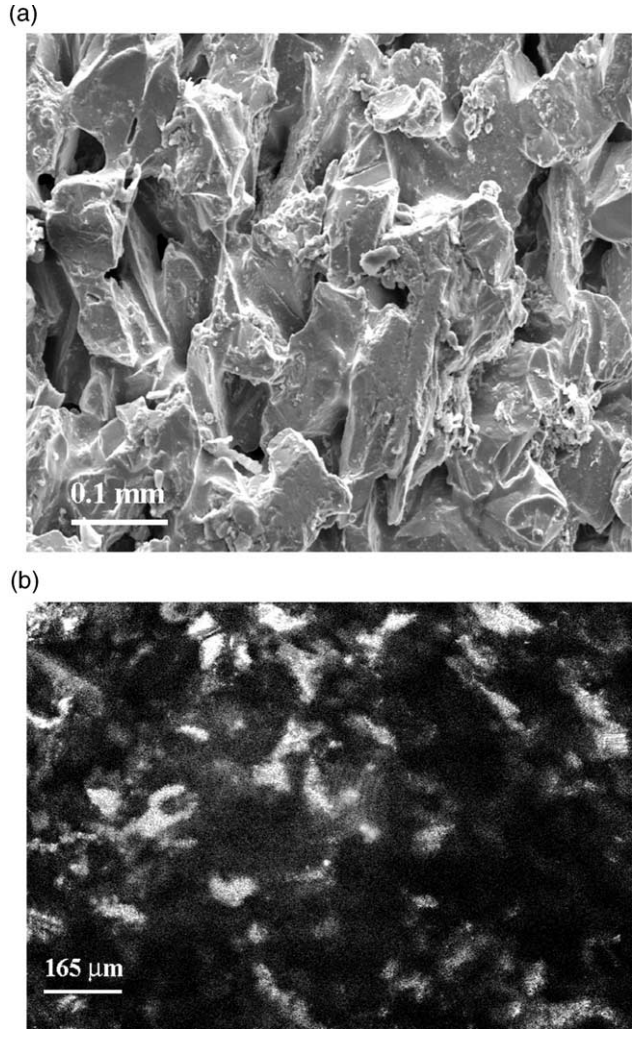

Fig. 10. The surface topography of the grinding wheel: (a) general view; (b) wear flats of the grinding wheel (at depth of cut=105 μm).

Table 5
Effect of the depth of cut on the wheel's wear flats and energy partition to workpiece

Depth of cut (μm)	Wear flats area (μm²)	Energy partition of the workpiece
35	13.8	0.864
70	14.3	0.866
105	15	0.869

where k_{ge} is the effective thermal conductivity of the alumina wheel, r_0 is the characteristic dimension of wear flats the alumina grinding wheel, v_s is the grinding wheel velocity, $\sqrt{(k\rho c)_w}$ is the thermal contact coefficient of the workpiece material. The results of partition ratio for different grinding conditions are presented in Table 5. The partition ratio is unchanged and appears to be 0.86 on average. This seems to indicate that the depth of cut does not influence the energy partition when the wheel and workpiece materials are given.

3.4. Contact length and elastic modulus of the grinding wheel

Using the l_a determined in Section 3.1 (i.e., l_a=1), the contact length of the heat flux (L_c) can be obtained by matching the experimental and theoretical widths of the heated zone. The results are presented in Table 6. The geometrical contact lengths are close to the calculated values when the infeed velocity and depth of cut are both low. The deviation from the geometrical contact length becomes pronounced when the infeed velocity and depth of cut are high. For example, at depth of cut of 105 μm and infeed velocity of 0.2 m/min the real contact length is 2.2 times larger than the geometrical value. The difference between the real and the geometrical contact lengths can be explained using Zhang's mechanical model [15], which states that the contact-deformation of the grinding wheel is an important factor that contributes the contact length increment. In this model the real contact length (L_c) is taken as:

$$L_c = R_d \arccos\left(1-\frac{d_c}{R_d}\right) \tag{3}$$

where d_c is the diameter of the grinding wheel and R_d is the equivalent wheel radius after deformation given by

$$R_d = R_0\left(1 + \zeta\frac{(1-\nu_s^2)F'_n}{E_s d_c}\right) \tag{4}$$

in which R_0 is the wheel radius before deformation, ζ is a constant determined by grinding conditions, ν_s is the Poisson's ratio of the wheel, F'_n is the normal grinding force per unit width, E_s is the macroscopic elastic modu-

Table 6
Experimental and theoretical contact lengths

Grinding regimes		Geometrical contact length (mm)	Calculated contact length (mm)
Depth of cut (μm)	Infeed velocity (m/min)		
35	0.02	3	N/A
	0.05		3
	0.1		3
	0.2		3
	0.3		3.9
70	0.02	4.4	4.40
	0.05		5.10
	0.1		6.46
	0.2		6.60
	0.3		6.50
105	0.02	5.4	5.4
	0.05		7.56
	0.1		9.72
	0.2		10.8
	0.3		9.1

lus of the wheel which is 40 GPa at room temperature [8]. The variation of E_s with grinding temperature can be determined using Eqs. (3 and (4)), and the experimentally measured F^1_n and calculated L_c. The results are shown in Fig. 11, where the thermal input, U, is defined as the product of the average surface temperature in the grinding zone and the contact length. The figure shows that the elastic modulus of the grinding wheel does not have a visible change when the thermal input (U) is less than a critical value. A further increase in the thermal input reduces the modulus quickly and the variation can be described by a simple power law as

$$E_s = kU^m \tag{5}$$

where k and m are constants to be determined by experiment.

If Eq. (5) is written in a dimensionless form, then

$$\frac{E_s}{E_0} = \tilde{k}\left(\frac{U}{wT_0}\right)^n \tag{6}$$

where E_0 is the wheel's elastic modulus at room temperature (40 GPa in this case), w is the grinding width (i.e., the contact width of the workpiece with the wheel, which is 15 mm in the present study) and T_0=800 °C is the temperature of α–γ phase transformation of the workpiece material. In this case, both $\tilde{k} = 0.076$ and n=−2.076 are non-dimensional. For grinding with a different wheel or workpiece material, $\tilde{k}$ and n will vary.

4. Conclusions

Using a new temperature measurement method and a contact mechanics model, this paper revisited some wheel–workpiece interaction problems in surface grinding and the following conclusions can be drawn:

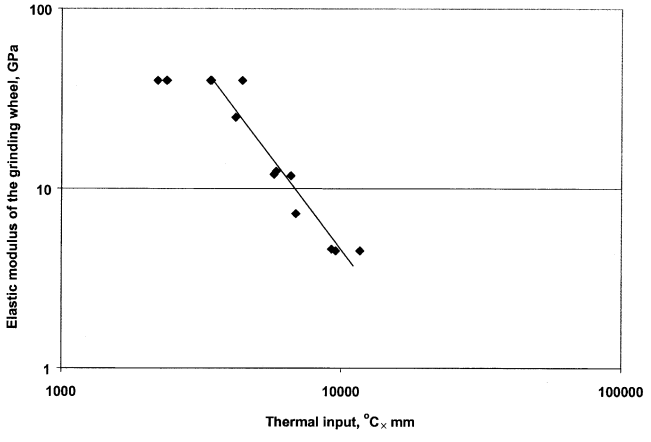

Fig. 11. The effect of the grinding temperature on the elastic modulus of the grinding wheel.

1. The heat flux in up-grinding can be theoretically modeled as a triangle with l_a =1. The model can predict well the heated zone in surface grinding.
2. The change of the elastic modulus of the grinding wheel is significant when the grinding temperature is beyond a critical value.
3. The variation of the modulus can be described by a simple power law.
4. Energy partition into wheel or workpiece is governed by their materials. With a given pair of wheel–workpiece material, the change of the depth of cut has almost no effect on the energy partition.
5. Unstable grinding heating can lead to a poor surface integrity.

Acknowledgements

The authors wish to thank the Australian Research Council (ARC) for continuing support of this project and the Electron Microscope Unit of Sydney University for use of its facilities.

References

[1] I. Zarudi, L.C. Zhang, Mechanical property improvement of quenchable steel by grinding, Journal of Materials Science (accepted for publication).
[2] M.C. Shaw, Temperatures in cutting and grinding, American Society of Mechanical Engineering 146 (1990) 17–24.
[3] A.S. Lavine, S. Malkin, T.C. Jen, Thermal aspects of grinding with CBN wheels, CIRP Annals 38 (1989) 557–560.
[4] C. Guo, S. Malkin, Analysis of energy partitions in grinding, Journal of Engineering for Industry 117 (1995) 55–61.
[5] L.C. Zhang, T. Suto, H. Noguchi, T. Waida, An overview of applied mechanics in grinding, Manufacturing Review 4 (1992) 261–273.
[6] L.C. Zhang, T. Suto, H. Noguchi, T. Waida, On some fundamental problems in grinding, in: Computer Methods and Experimental Measurement for Surface Treatment Effects, Proceedings of the First International Conference on Computer Methods and Experimental Measurements for Surface Treatment Effects, Computational Mechanics Publications, Southampton, 1996, pp. 275–284.
[7] M. Mahdi, L. Zhang, Applied mechanics in grinding—VI. Residual stresses and surface hardening by coupled thermo-plasticity and phase transformation, International Journal of Machine Tools & Manufacture 38 (1998) 1289–1304.
[8] L.C. Zhang, T. Suto, H. Noguchi, T. Waida, Applied mechanics in grinding. Part II: Modelling of elastic modulus of wheel and interface forces, International Journal of machine Tools & Manufacture 33 (1993) 245–255.
[9] C. Guo, Y. Wu, V. Varghese, S. Malkin, Temperatures and energy partition for grinding with vitrified CBN wheels, Annals of CIRP 42 (1999) 247–250.
[10] W.B. Rowe, S.C. Black, B. Mills, H.C. Qi, M.N. Morgan, Experimental investigation of heat transfer in grinding, Annals of CIRP 44 (1995) 329–332.
[11] T.C. Jen, A.S. Lavine, A variable heat flux model of heat transfer in grinding: model development, Journal of Heat Transfer 117 (1995) 473–478.

[12] A.S. Lavine, T.C. Jen, Thermal aspects of grinding: heat transfer to workpiece, wheel and fluid, ASME Journal of Heat Transfer 113 (1991) 296–303.
[13] C. Guo, S. Malkin, Inverse heat transfer analysis of grinding. Part 2: Applications, Journal of Engineering for Industry 118 (1996) 143–149.
[14] J. Jaeger, Moving sources of heat and the temperature at sliding contacts, Journal and Proc. of the Royal Society of NSW 76 (1942) 203–224.
[15] L.C. Zhang, T. Suto, H. Noguchi, T. Waida, Applied mechanics in grinding, Internatinal Journal of Machining Tools & Manufacture 33 (1993) 587–597.